Metals and Materials International (2021) 27:425–435
https://doi.org/10.1007/s12540-019-00561-3

Hydrogen Behavior in Ti-Added Reduced Activation Ferritic-Martensitic Steels

Kang-Mook Ryu[1] · Dae Geon Lee[1] · Joonoh Moon[2] · Chang-Hoon Lee[2] · Tae-Ho Lee[2] · Jae Sang Lee[1] · Dong-Woo Suh[1]

Received: 12 November 2019 / Accepted: 22 November 2019 / Published online: 5 December 2019

Abstract

Hydrogen behavior and corresponding mechanical degradation were examined in TaTi-RAFM and EUROFER97 steels. Increased Ta content with Ti addition decelerates the hydrogen diffusion but increases the solubility in the lattice. It is mainly led by the higher fraction of Ta-rich MC carbides and dislocation density in TaTi-RAFM steel. Overall activation energy of hydrogen trapping of investigated steels is evaluated to be 25.3 ~ 25.6 kJ/mol in the tempered condition. The activation energy increases to nearly 30 kJ/mol when the steels are re-austenitized and quenched. Higher activation energy with increased dislocation density indicates that the dislocation provides for trap site with higher activation energy than Ta-rich MC carbide. Mechanical degradation by hydrogen with respect to the yield strength, tensile strength and uniform elongation could not be observed in all investigated steels. The presence of hydrogen only has influence on the loss of post-uniform elongation. For a given charging time, the loss of post-uniform elongation is more remarkable in TaTi-RAFM steel due to the larger hydrogen uptake.

Graphic Abstract

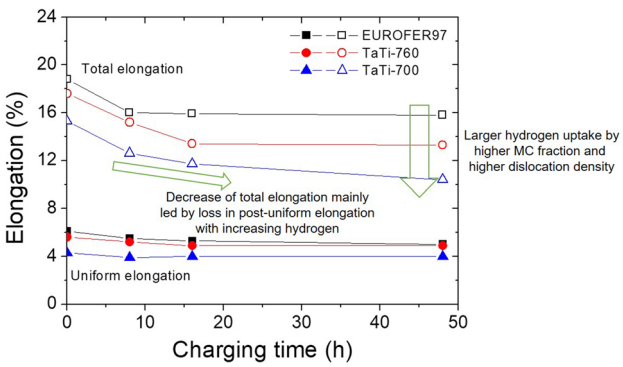

Keywords RAFM steel · Hydrogen · Diffusion · Ta-rich carbide · Dislocation

1 Introduction

Nuclear fusion is attracting a great attention as a promising energy solution for the next generation [1]. The blanket, which is one of the most important components in the fusion reactor, is placed on inside wall of reactor and plays a key role in converting high-speed neutrons into thermal energy, supplying tritium through nuclear fission of lithium and isolating the plasma in the reactor. The materials for blanket need low activation properties as well as strength and toughness

✉ Dong-Woo Suh
dongwoo1@postech.ac.kr

[1] Graduate Institute of Ferrous Technology, POSTECH, Pohang 37673, Republic of Korea

[2] Ferrous Alloy Department, Korea Institute of Material Science, Changwon 51508, Republic of Korea

at high temperature [2]. Besides, since hydrogen isotopes are main resource for fusion reaction, a high resistance to hydrogen embrittlement is also required for the blanket exposed to hydrogen in service. Considering these environments, reduced activation ferrite martensite (RAFM) steels have been regarded as the most prospective material for the blanket among a variety of candidates [3, 4]. The chemistry of RAFM steels are close to the conventional 9% Cr-containing heat resistant steel, but W and Ta are added instead of high activation elements such as Mo and Nb.

There have been several reports on the influence of hydrogen on the RAFM steels. Most of the studies tried to evaluate the hydrogen diffusion parameters or the mechanical degradation in RAFM steel at the presence of hydrogen. For instance, Esteban et al. [5, 6] reported the hydrogen diffusion parameters of various RAFM steel including EUROFER97 through a gas evolution permeation technique at high temperature. Aiello et al. [7] examined hydrogen diffusivity in EUROFER97 at room temperature using Devanathan cell. Yagodzinskyy et al. [8] evaluated the influence of hydrogen on the tensile properties of EUROFER97 and ODS-EUROFER97, and Beghini et al. [9] investigated threshold hydrogen contents on brittle fracture of F82H martensitic steel using low strain rate tests of notched specimens. Recently, Lee et al. [10–13] in Korea Institute of Material Science (KIMS) has developed TaTi-RAFM steel. By controlling Ta content with addition of Ti, fine (Ta, Ti, W)C precipitates are formed in the matrix, resulting in an excellent combination of strength and toughness. Although basic mechanical properties such as high temperature strength or DBTT have been evaluated, the hydrogen-related characteristics have not been systematically examined for the newly developed TaTi-RAFM steel. Therefore, the purpose of present study is to investigate the hydrogen diffusion parameters in the TaTi-RAFM steel and the mechanical performance at the presence of hydrogen. In particular, it is attempted to understand the characteristics of hydrogen behavior in the TaTi-RAFM steel with respect to the microstructure features influenced by Ta and Ti content.

2 Experimental

2.1 Materials

The chemical compositions of investigated steels are presented in Table 1. EUROFER97, a traditional RAFM steel, as well as TaTi-RAFM steel is considered for comparative study. The TaTi-RAFM steel contains Ti by 0.01–0.015 wt% with increased Ta content compared to the EUROFER97; it was reported to refine the microstructure and introduce high density of nano-sized Ta-rich MC (M = Ta, V, Ti) precipitation in the TaTi-RAFM steel, resulting in excellent high temperature strength, toughness (low DBTT) and creep strength [11].

Both RAFM steels were heat-treated using reported practices. The EUROFER97 was normalized at 980 °C for 30 min and tempered at 760 °C for 90 min. The TaTi-RAFM was tempered at 760 °C and 700 °C respectively, after normalizing at 1000 °C. In the present study, TaTi-RAFM steels were designated as TaTi-760 and TaTi-700 according to the tempering condition.

2.2 Hydrogen Permeation Test

A hydrogen permeation test was conducted using Devanathan-Stachursky cell at room temperature to evaluate hydrogen diffusion parameters. Hydrogen is electrochemically charged in an aqueous solution containing 3 wt% sodium chloride and 0.3 wt% ammonium thiocyanate at a cathodic current density of 1.5 mA/cm^2 [14–16]. The current density on the detecting cell gradually increases and then becomes nearly constant at steady state. Hydrogen diffusion parameters such as diffusivity, solubility and permeability can be determined from the permeation curve. The steady state hydrogen permeation flux is converted to the permeability (mol s^{-1} m^{-1}) according to following Eq. (1) [17].

$$\Phi = \frac{I_\infty \cdot L}{nF} \tag{1}$$

where I_∞ is the steady state current density, n is the number of electrons participated in the electrochemical reaction, F is Faraday constant and L is the thickness of specimen.

The effective hydrogen diffusivity (m^2 s^{-1}) is calculated from the time-lag method (Eq. 2).

$$D_{eff} = \frac{L^2}{6 \cdot t_{lag}} \tag{2}$$

where t_{lag} is time lag defined to be that required to achieve 0.63 of the steady-state current density in the permeation curve. Then, hydrogen solubility (mol m^{-3}) can be evaluated by following Eq. (3).

$$S = \frac{\Phi}{D_{eff}} \tag{3}$$

Table 1 Chemical composition of tested specimens (in wt%)

Materials	C	Si	Mn	Cr	V	W	Ta	Ti
EUROFER97	0.09	0.14	0.36	9.0	0.20	1.0	0.035	–
TaTi-RAFM	0.09	0.06	0.40	9.1	0.21	1.0	0.092	0.012

2.3 Thermal Desorption Analysis

Thermal desorption analysis was performed to examine the hydrogen uptake and trapping characteristics. Hydrogen was electrochemically charged into the specimens in an aqueous solution with 3 wt% sodium chloride and 0.3 wt% ammonium thiocyanate at the current density of 10 mA/cm^2 [18]. The hydrogen desorption was monitored with gas chromatography at a constant heating rate of 100, 200 and 300 °C/h up to 300 °C. Detrapping activation energy was estimated using Kissinger's formula (Eq. 4) [19].

$$\frac{\partial \ln\left(\varphi/T_p^2\right)}{\partial\left(1/T_p\right)} = -\frac{E_a}{R} \tag{4}$$

where φ is the heating rate (K/min), T_p is the peak temperature of thermal desorption spectra (K), E_a is the detrapping activation energy (kJ/mol) and R is the gas constant (kJ/mol K).

2.4 Slow Strain Rate Tensile Test

Slow strain tensile tests were conducted to evaluate the susceptibility to hydrogen-induced mechanical degradation. Sub-sized specimens with 4 mm-diameter and 25 mm-gauge length were prepared in compliance with ASTM E8. The specimen was electrochemically charged with hydrogen in an aqueous solution at the current density of 10 mA/cm^2, and then was Zn-coated to avoid the hydrogen effusion during testing. The test was conducted at a nominal strain rate of 10^{-5} s^{-1}. A loss of elongation was evaluated by Eq. (5) as an index of hydrogen susceptibility.

$$\mathrm{El}_{\mathrm{Loss}}(\%) = \frac{\mathrm{El}_{\mathrm{H\,free}} - \mathrm{El}_{\mathrm{H\,charged}}}{\mathrm{El}_{\mathrm{H\,free}}} \times 100 \tag{5}$$

2.5 Microstructural Characterization

Detailed microstructural characterization was performed using scanning electron microscopy and transmission electron microscopy. Samples for SEM examination were etched using 1% picric solution (1 g picric acid + 5 ml HCl + 100 ml ethyl alcohol). Thin foils for TEM examination were mechanically ground down to 100 μm in thickness, and electro-polished in 95% acetic acid and 5% perchloric acid using twin-jet electro-polisher at ambient temperature. Carbon extraction replica samples for quantitative analysis of precipitation were prepared using electro-polishing in 8% HCl and 92% methanol electrolyte at 1 V. The amount of alloying element participating to the precipitation was evaluated using selective chemical dissolution method [20].

3 Results and Discussion

3.1 Microstructure and Tensile Properties

As shown in Fig. 1, the microstructure of heat treated RAFM steels is mainly covered with tempered martensite matrix with precipitates. Detailed observation using TEM reveals rather coarse precipitates along the boundaries and tiny precipitates in the matrix (Fig. 2). It was reported in the earlier study that Cr-rich $M_{23}C_6$ carbide precipitated at grain boundary and Ta-rich MC carbide evolved in the lath in typical RAFM steels [10, 21–23]. Equilibrium fraction of precipitation calculated by Thermo-Calc with TCFE7 database shows that the fraction of $M_{23}C_6$ is similar in EUROFER97 and TaTi-RAFM steels but the fraction of MC carbide is nearly 3 times larger in TaTi-RAFM steel (Fig. 3); it is led by increased Ta content and Ti addition. Table 2 shows the results of selective chemical dissolution analysis, indicating amount of carbide forming elements participating to the precipitation. It is noted that Ta or Ti readily precipitates as carbides compared to Cr or W. Moreover, Ta is more actively involved in carbide in the TaTi-RAFM steel. It accords with the report by Kim et al. that the addition of Ti with Ta accelerates the kinetics of MC precipitation [13]. Even with slightly higher normalizing temperature, the size of prior austenite grain in TaTi-RAFM (10 ~ 15 μm) is finer compared to that in EUROFER97 (25 μm) (Fig. 4); it is possibly attributed to the higher fraction of fine MC carbide [24].

Dissimilar precipitation behavior also affects the tensile properties (Table 3). Yield and tensile strength of TaTi-RAFM steel are higher than those of EUROFER97. Indeed, the strength could be improved with a marginal loss of elongation at the same tempering condition (760 °C). It is probably led by precipitation hardening with MC carbides in TaTi-RAFM steel. But smaller prior austenite grain size and the presence of tiny precipitates also affect the density and annihilation of dislocation in the course of normalizing and tempering. Lower tempering temperature (700 °C) in TaTi-RAFM steel remarkably increases the strength at the expense of elongation, ascribed to the sluggish dislocation annihilation.

3.2 Hydrogen Behavior

The hydrogen permeation curves of investigated steels are given in Fig. 5. The vertical axis of the graph represents the current density normalized over steady state condition. The horizontal axis is the lead-time divided by the square of thickness of the specimens in order to obtain the permeation

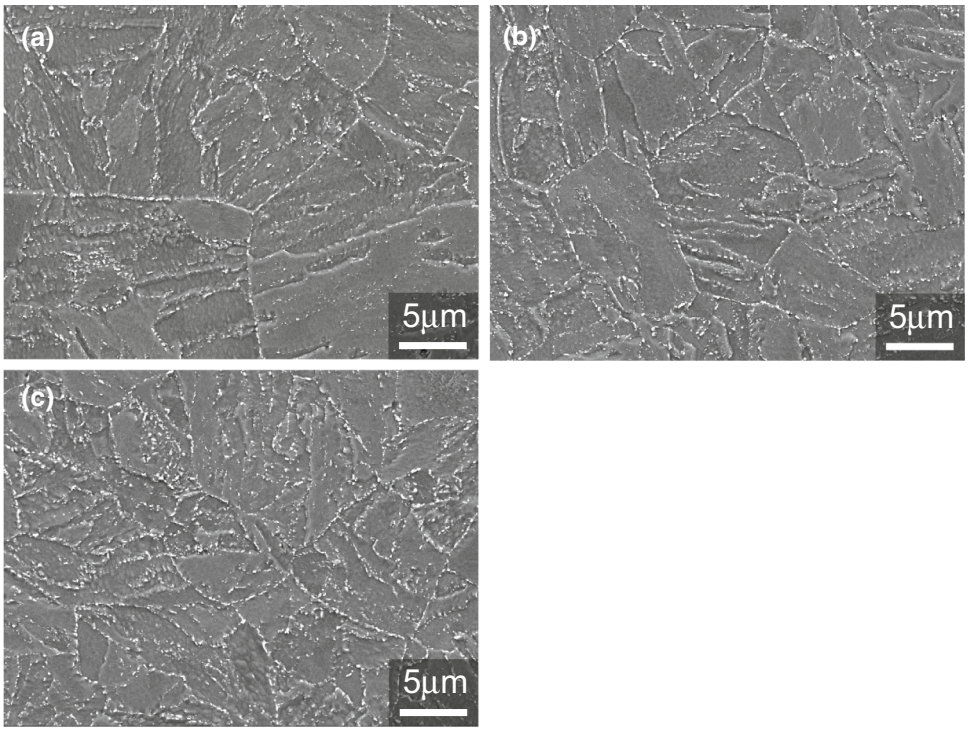

Fig. 1 SEM micrographs of **a** EUROFER97, **b** TaTi-760 and **c** TaTi-700

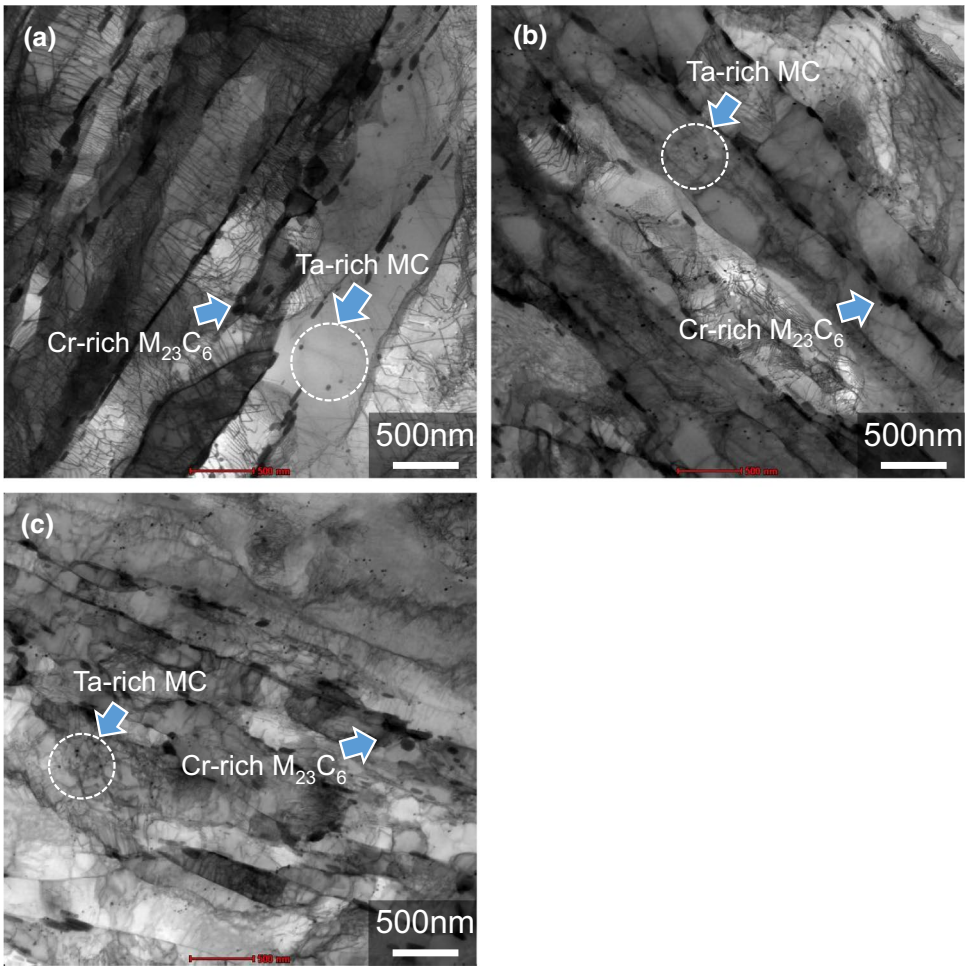

Fig. 2 TEM micrographs of **a** EUROFER97, **b** TaTi-760 and **c** TaTi-700

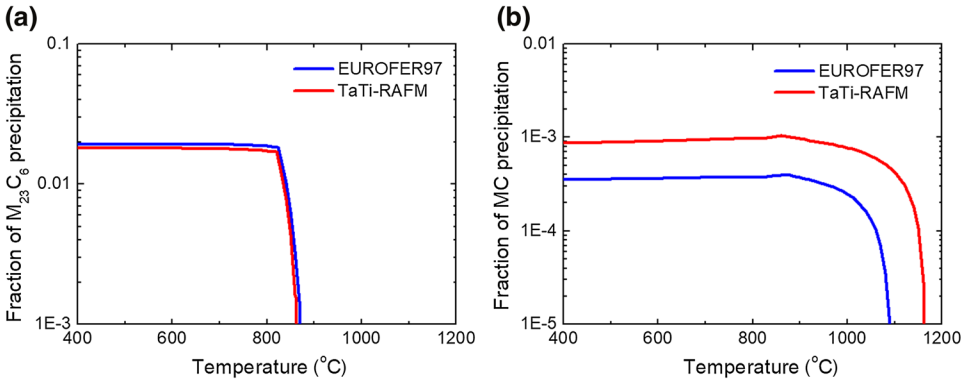

Fig. 3 Equilibrium fraction of **a** $M_{23}C$ and **b** MC carbide

Table 2 Amount of alloying elements participating to the precipitates (wt%). Number in the parenthesis presents the ratio of element in the precipitate

	Cr	W	Ta	Ti
EUROFER97	0.65 (7.2%)	0.11 (10.8%)	0.026 (73.3%)	–
TaTi-760	0.73 (8.1%)	0.17 (16.5%)	0.080 (86.7%)	0.0046 (38.6%)
TaTi-700	0.77 (8.5%)	0.17 (16.0%)	0.079 (86.2%)	0.0044 (37.1%)

flux excluding the thickness effect. The hydrogen diffusion parameters evaluated from the permeation curves indicate that the apparent diffusivity is decreased in following order: EUROFER97, TaTi-760 and TaTi-700, and the solubility is in a reverse order (Table 4). The diffusion parameters are closely related to the density of the hydrogen trap sites because the interaction of hydrogen with the trap sites decelerates the mobility but increases the solubility of hydrogen in the lattice. Considering the microstructure of RAFM steels, various types of trap sites will contribute to the hydrogen behavior: dislocations, interfaces and precipitates. As mentioned, the fraction of MC carbide in TaTi-RAFM steel is higher than that in EUROFER97. It will have a significant trapping effect, resulting in slower diffusivity in TaTi-RAFM steel. Nevertheless, it cannot be ruled out that other trap sites such as dislocation have an influence on the hydrogen behavior as well.

More detailed understanding on the interaction between trap sites and hydrogen can be obtained using thermal desorption analysis. Thermal desorption rate of hydrogen gradually increases with charging time and a single peak is detected in temperature ranging 80 ~ 100 °C (Fig. 6). The amount of hydrogen as a function of charging time (Fig. 7) indicates that hydrogen uptake is saturated over 8 h, 16 h and 32 h for EUROFER97, TaTi-760 and TaTi-700, respectively. The TaTi-700 steel exhibits the highest saturation level and then TaTi-760, EUROFER97. The time for hydrogen saturation and the amount of total hydrogen contents accord well with the diffusion parameters derived from the hydrogen permeation test, indicating slower diffusion but

Table 3 Tensile Properties of heat treated RAFM steels

Strain rate, s^{-1}		YS, MPa	TS, MPa	El., %
10^{-3}	EUROFER97	493	621	21.0
	TaTi-760	523	639	19.0
	TaTi-700	611	711	15.7

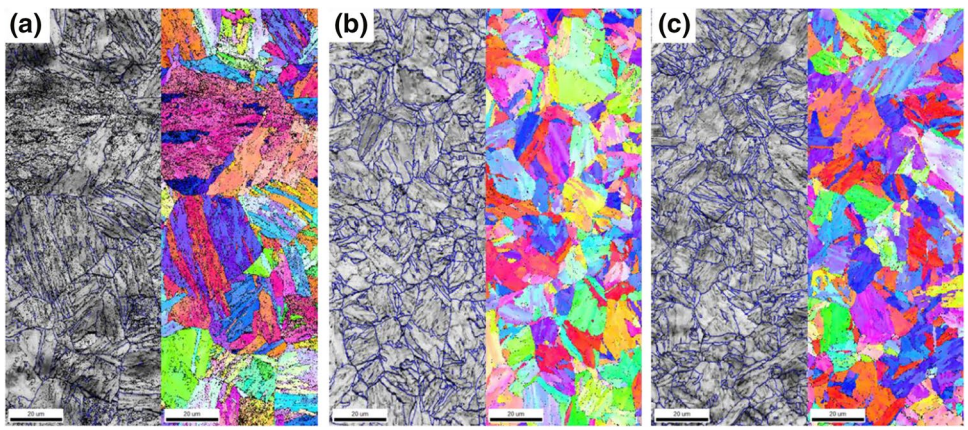

Fig. 4 EBSD map of **a** EUROFER97, **b** TaTi-760 and **c** TaTi-700 (Blue line indicates the high angle boundary of which misorientation angle is higher than 15°). (Color figure online)

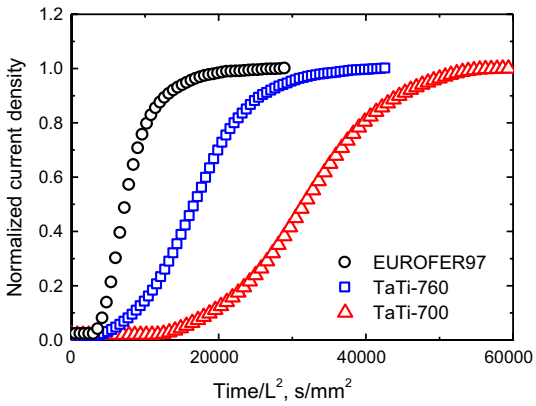

Fig. 5 Hydrogen permeation curves

Table 4 Hydrogen diffusion parameters

	Permeability (mol s^{-1} m^{-1})	Diffusivity (m^2 s^{-1})	Solubility (mol m^{-3})
EUROFER97	5.24×10^{-10}	2.01×10^{-11}	26.03
TaTi-760	7.33×10^{-10}	9.17×10^{-12}	79.90
TaTi-700	4.23×10^{-10}	4.82×10^{-12}	87.86

higher solubility of hydrogen in TaTi-RAFM steels. The activation energy for hydrogen effusion from the trap site (E_a) can be estimated by analyzing the peak temperature of thermal desorption rate at various heating rates using Eq. (4). Analysis on a series of desorption curves presents that E_a of investigated steels is around 25.3 ~ 25.6 kJ/mol (Fig. 8 and Table 5). It is noted that the E_a reflects the overall response from several types of trap sites in the lattice. Earlier studies disclosed that the detrapping activation energy of hydrogen from dislocation or lath boundary of martensite is in range of 20 ~ 30 kJ/mol [25–29]. On the other hand, in case of precipitates, coherency with matrix is reported to affect the activation energy. For instance, E_a of TiC precipitate was estimated to be 40 ~ 116 kJ/mol depending on its coherency with matrix [26, 28, 30, 31]. Incoherent TiC presents very strong hydrogen trapping ability as an irreversible trap site. In addition, E_a of coherent NbC was reported to be 23 ~ 48 kJ/mol and that of incoherent NbC appeared to be in range between 63 and 68 kJ/mol [32]. Even though there are considerable scatters in the reported detrapping activation energies, the precipitation such as TiC or NbC is thought to provide a stronger trap site for hydrogen than dislocation or lath boundary of martensite. However, the major precipitate in the TaTi-RAFM steel is Ta-rich MC carbide, which differs in chemistry from Ti or Nb based MC carbide. Therefore, it is necessary to examine detailed hydrogen trapping behavior in the RAFM steel.

As a way to evaluate the relative hydrogen trapping ability between dislocation and MC precipitation which can be considered important hydrogen trap sites, we compared the hydrogen behaviors in the tempered RAFM steels with

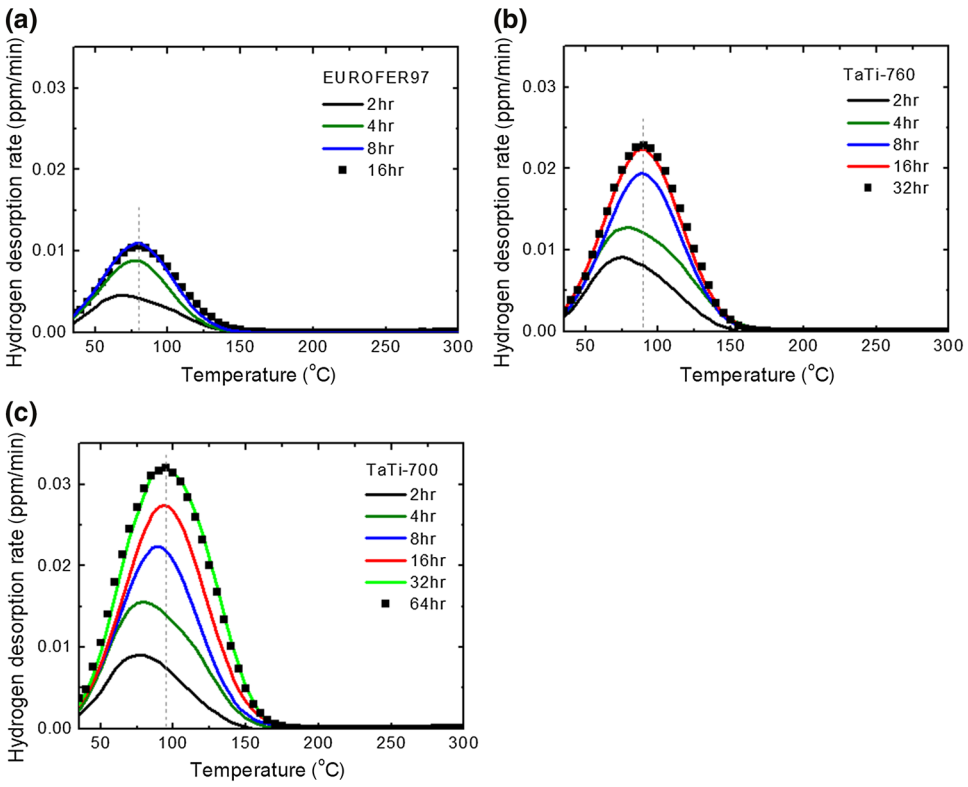

Fig. 6 Thermal desorption curves of **a** EUROFER97, **b** TaTi-760 and **c** TaTi-700

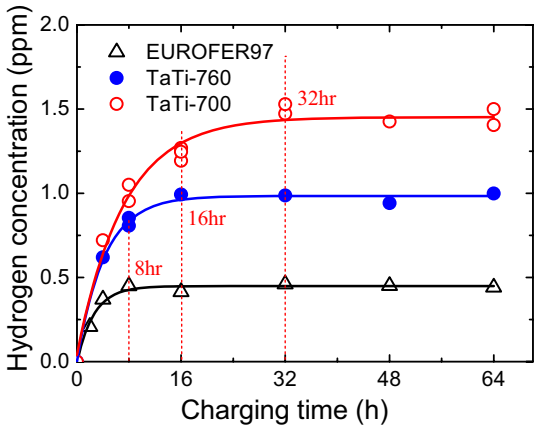

Fig. 7 Diffusible hydrogen content with charging time

re-austenitized at normalizing temperature and quenched ones. According to the thermodynamic calculation, approximately 70% and 90% of MC carbide is still undissolved in EUROFER97 and TaTi-RAFM steel, respectively, meanwhile the dislocation density is expected to increase in as-quenched condition with nearly the same martensitic lath structure. Accordingly, any change in the hydrogen uptake and detrapping activation energy will be associated with the relative trapping ability of dislocation and Ta-rich MC carbide. Figure 9 compares the thermal desorption spectrum of tempered and as-quenched steels. The hydrogen uptake is enhanced in the as-quenched steel at the same charging condition. Analysis on XRD profiles using modified

Table 5 Hydrogen detrapping activation energy

Materials	E_a (kJ/mol)	
	Tempered	As-quenched
EUROFER97	25.4	30.5
TaTi-760	25.8	30.7
TaTi-700	26.5	

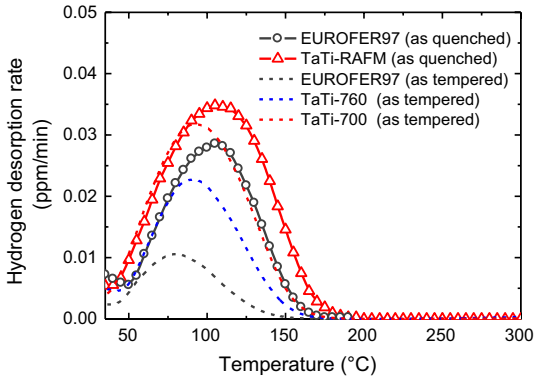

Fig. 9 Thermal desorption curves of investigated RAFM steel with various heat treatment conditions

Williamson-Hall and Warren–Averbach method [33, 34] reveals higher dislocation density in as-quenched conditions (Fig. 10a) and the amount of hydrogen content is mostly proportional to the dislocation density (Fig. 10b); it indicates that the increase of the dislocation density mainly

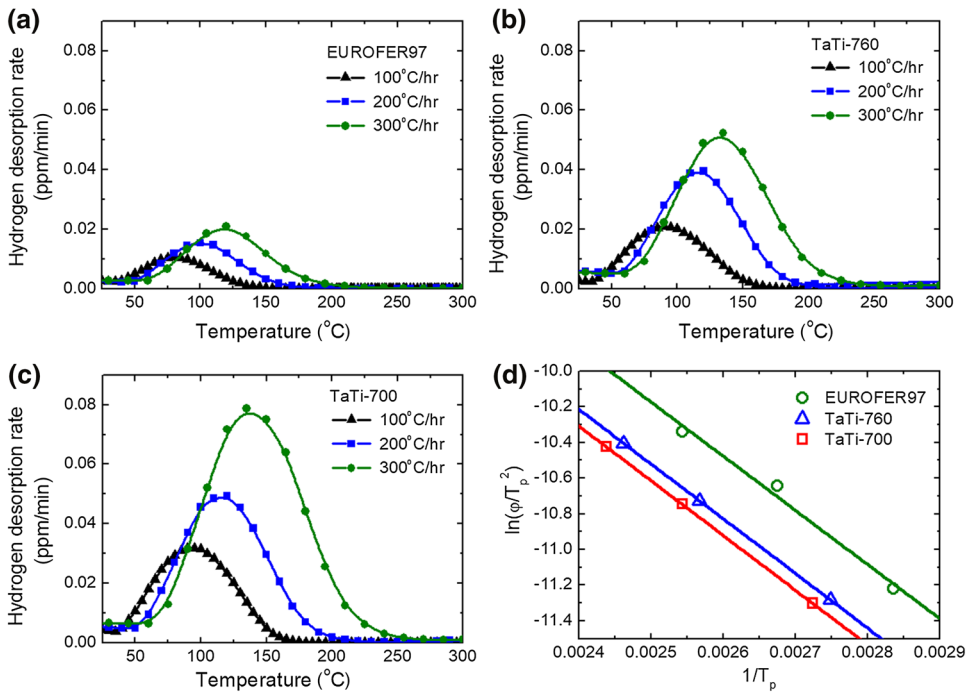

Fig. 8 Thermal desorption curves of **a** EUROFER97, **b** TaTi-760 and **c** TaTi-700 at different heating rate, and **d** Kissinger plot to obtain detrapping activation energy

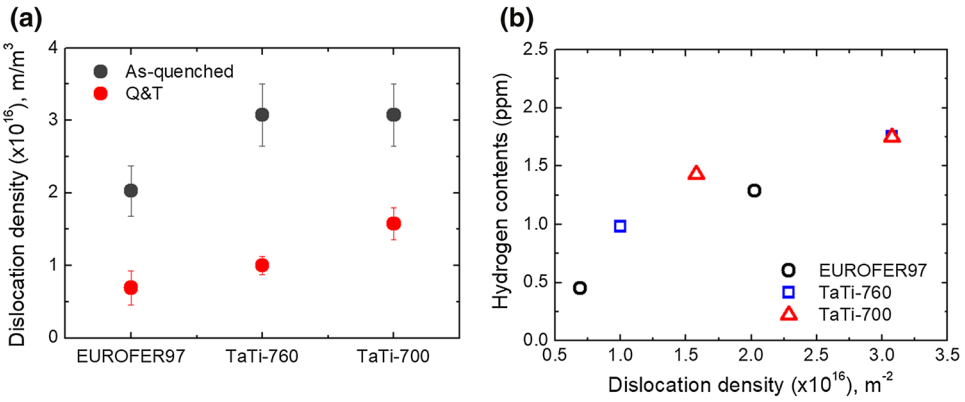

Fig. 10 **a** Dislocation density and **b** hydrogen content with dislocation density

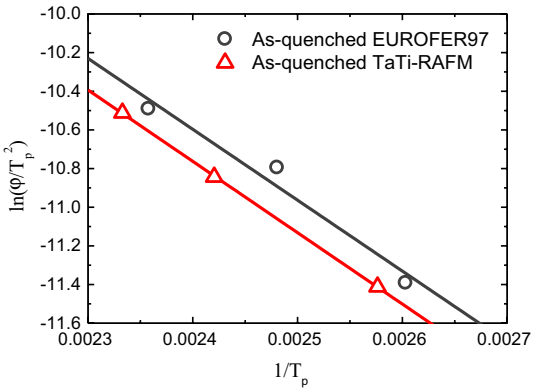

Fig. 11 Kissinger plot to obtain detrapping activation energy in as-quenched RAFM steels

contributes to the enhancement of hydrogen uptake in the as-quenched steel. Figure 11 illustrates the analysis on overall detrapping activation of hydrogen for the as-quenched steels from the peak temperature of thermal desorption rate at various heating rates and the results are summarized in Table 5. It is noteworthy that the detrapping activation energy of hydrogen is higher for as-quenched condition compared to that for the tempered one. Since the increase of dislocation density is thought to affect more significantly on the change of hydrogen trapping characteristics after quenching, higher detrapping energy in as-quenched condition implies that the dislocation is more intensively interacting with hydrogen than Ta-rich MC carbide. This is interesting result because it has been commonly reported that the Ti, Nb or V based MC carbides provide stronger trap site for hydrogen than dislocation or grain boundary, so that they can be used for alleviating hydrogen-related mechanical degradation. However, given that the trap ability is strongly dependent on the species of carbide forming element, it is not surprising that Ta-rich MC carbide is expected to have rather lower detrapping activation energy than the dislocation. Nevertheless, further investigation on the interaction between hydrogen and Ta-rich MC carbide is thought to be necessary.

3.3 Susceptibility to Mechanical Degradation by Hydrogen

Figure 12 presents the stress–strain curves of RAFM steels using slow strain tensile test. It is recognized that all RAFM steels exhibit mechanical degradation in terms of total elongation loss as the hydrogen charging time increases. At saturated hydrogen charging condition of 48 h, total elongation loss is evaluated to be 16.0%, 24.2% and 32.3% for EUROFER97, TaTi-760 and TaTi-700 steel respectively. It appears that the TaTi-RAFM steel is more sensitive to the mechanical degradation by hydrogen. However, a closer look on the total elongation loss as a function of hydrogen content (Fig. 13) clearly indicates that all RAFM steels investigated in the present study have similar hydrogen susceptibility at a given hydrogen content; it is insensitive to the chemistry or the tempering condition. Indeed, more hydrogen uptake is required in TaTi-RAFM steel than EUROFER97 to arise similar level of mechanical degradation; for instance, hydrogen content more than 0.8 ppm is necessary for total elongation loss around 15% in TaTi-RAFM steel but only a half of hydrogen uptake can cause similar level of degradation in EUROFER97. Besides, it is noted there is little mechanical degradation regarding to the tensile strength; in other words, the uniform elongation is hardly affect by the presence of hydrogen. Considering that the post-uniform elongation is less significant with respect to the engineering application, a conservation of yield, tensile strength and uniform elongation at saturated hydrogen level suggests that RAFM steels investigated in the present study are robust against to the hydrogen-induced mechanical degradation. In particular, it is noteworthy that the TaTi-RAFM steel exhibits nearly the same hydrogen susceptibility to the EUROFER97 even with higher strength.

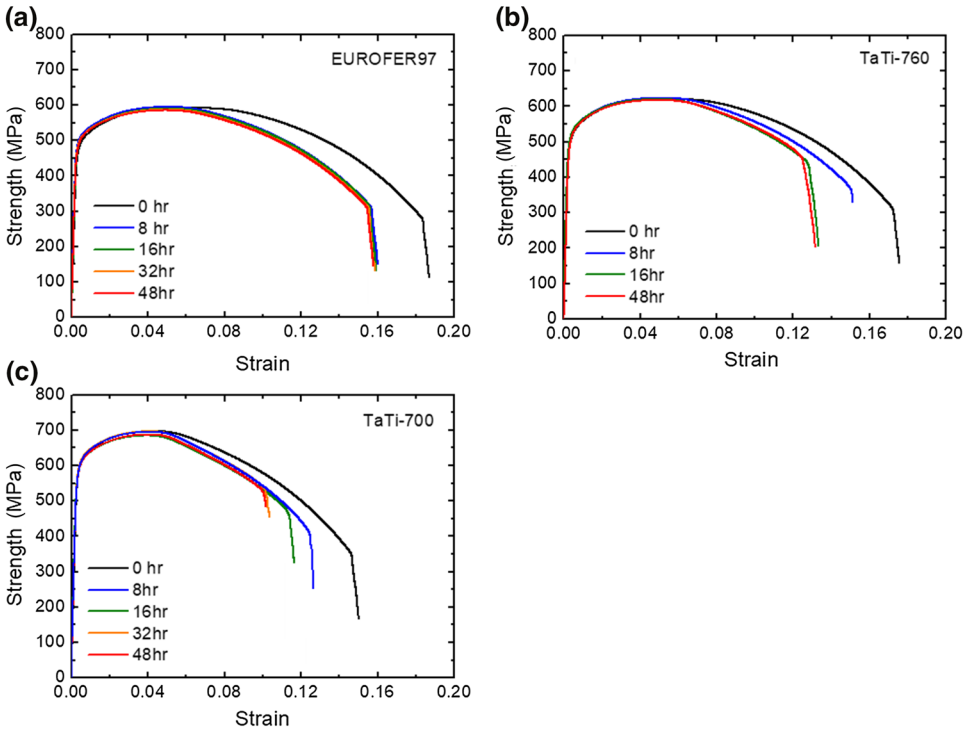

Fig. 12 Stress-strain curves obtained using slow strain tensile test of **a** EUROFER97, **b** TaTi-760 and **c** TaTi-700

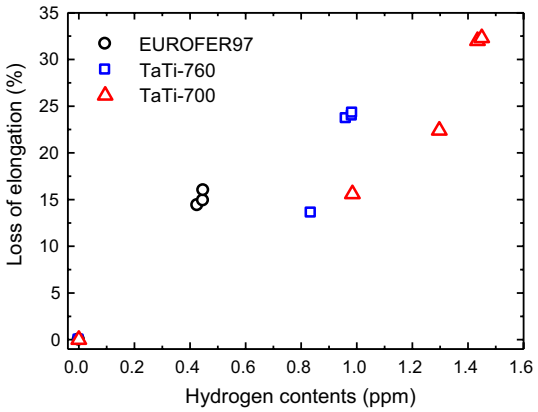

Fig. 13 Loss of total elongation with diffusible hydrogen content

The loss of total elongation is mainly led by the decrease in the post-uniform elongation. It represents that the mechanical degradation by hydrogen is limited to the deformation related to the necking following the uniform elongation; therefore the increased Ta content with Ti addition in the TaTi-RAFM steel has a beneficial influence on the improvement of strength without an increase of hydrogen susceptibility. The fracture surface of RAFM steels after SSRT indicates a ductile fracture with many micro-dimples (Fig. 14), which is consistent with the negligible loss of ductility in the investigated steels. Since the necking subsequent to the uniform elongation proceeds with the formation and coalescence of micro-voids, the loss of post-uniform elongation at a presence of hydrogen possibly implies that micro-voids are readily nucleated adjacent to the interface between the matrix and second phase. In that sense, the TaTi-RAFM steel will have a propensity for rapid nucleation of micro-void compared to the EUROFER97 because of the higher population of Ta-rich MC carbides and larger hydrogen uptake for a given charging time. That will be why the TaTi-RAFM steel exhibits more loss of post-uniform elongation at a given charging time compared to the EUROFER97.

4 Conclusion

Hydrogen behavior and corresponding mechanical degradation in TaTi-RAFM steel is investigated in the present study and following conclusions can be drawn.

(1) Increased Ta content with Ti addition in TaTi-RAFM steel decreases the hydrogen diffusion but increases the hydrogen solubility compared to EUROFER97.
(2) Overall activation energy of hydrogen trapping of investigated steels is evaluated to be 25.3 ~ 25.6 kJ/mol in the tempered condition. The activation energy increases to 30 kJ/mol when the steels are re-austen-

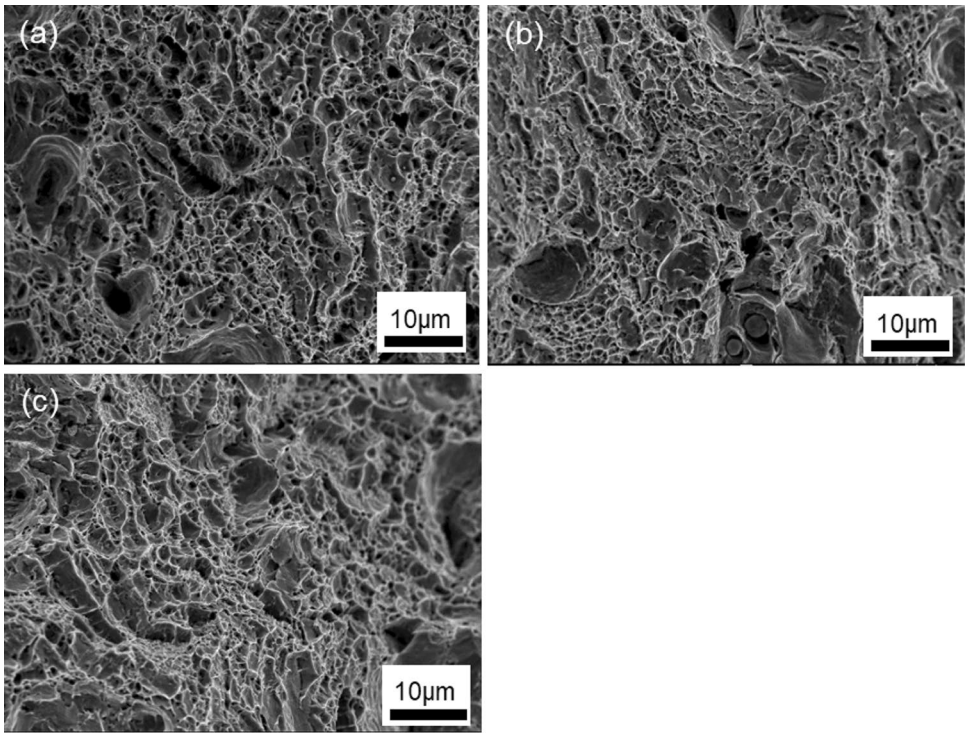

Fig. 14 Fracture surface after slow strain tensile test of **a** EUROFER97, **b** TaTi-760 and **c** TaTi-700

itized and quenched. It indicates that the dislocation more intensively interacts with hydrogen than Ta-rich MC carbide.

(3) Increased Ta content with Ti addition hardly causes the mechanical degradation regarding to the yield strength, tensile strength and uniform elongation even with enhanced strength level. The presence of hydrogen only affects the loss in the post-uniform elongation, which is more remarkable in TaTi-RAFM steel due to higher hydrogen uptake for a given charging time.

Acknowledgements This work was supported financially by the Fundamental Research Program of the Korea Institute of Materials Science (POC3380)

References

1. V. Barabash, T.I.I. Team, A. Peacock, S. Fabritsiev, G. Kalinin, S. Zinkle, A. Rowcliffe, J.-W. Rensman, A. Tavassoli, P. Marmy, J. Nucl. Mater. **367**, 21–32 (2007)
2. D. Steiner, Nuclear Applications and Technology **9**, 83–92 (1970)
3. Y. Wu, J. Nucl. Mater. **386**, 122–126 (2009)
4. S.J. Zinkle, J.T. Busby, Mater. Today **12**, 12–19 (2009)
5. G. Esteban, A. Perujo, K. Douglas, L. Sedano, J. Nucl. Mater. **281**, 34–41 (2000)
6. G. Esteban, A. Pena, I. Urra, F. Legarda, B. Riccardi, J. Nucl. Mater. **367**, 473–477 (2007)
7. A. Aiello, I. Ricapito, G. Benamati, R. Valentini, Fusion Sci. Technol. **41**, 872–876 (2002)
8. Y. Yagodzinskyy, E. Malitckii, M. Ganchenkova, S. Binyukova, O. Emelyanova, T. Saukkonen, H. Hänninen, R. Lindau, P. Vladimirov, A. Moeslang, J. Nucl. Mater. **444**, 435–440 (2014)
9. M. Beghini, G. Benamati, L. Bertini, I. Ricapito, R. Valentini, J. Nucl. Mater. **288**, 1–6 (2001)
10. C.-H. Lee, J. Moon, M.-G. Park, T.-H. Lee, M.-H. Jang, H.C. Kim, D.-W. Suh, J. Nucl. Mater. **455**, 421–425 (2014)
11. C.-H. Lee, J.-Y. Park, W.-K. Seol, J. Moon, T.-H. Lee, N.H. Kang, H.C. Kim, Fusion Eng. Des. **124**, 953–957 (2017)
12. J. Heo, S. Kim, H. Guim, H.-H. Jin, J. Moon, C.-H. Lee, C. Shin, J. Nucl. Mater. **512**, 184–192 (2018)
13. H.K. Kim, J.W. Lee, J. Moon, C.H. Lee, H.U. Hong, J. Nucl. Mater. **500**, 327–336 (2018)
14. M. Devanathan, Z. Stachurski, Proc. R. Soc. Lond. A **270**, 90–102 (1962)
15. N. Boes, H. Züchner, J. Less Common Met. **49**, 223–240 (1976)
16. S.J. Kim, H.S. Seo, K.Y. Kim, Met. Mater. Int. **21**, 666–672 (2015)
17. E. ISO, Method of measurement of hydrogen permeation and determination of hydrogen uptake and transport in metals by an electrochemical technique. Brussels: European Committee for Standardization
18. D. Kim, G.H. Jang, T. Lee, C.S. Lee, Met. Mater. Int. (2019). https://doi.org/10.1007/s12540-019-00514-w
19. H.E. Kissinger, Anal. Chem. **29**, 1702–1706 (1957)
20. J. Lu, J.B. Wiskel, O. Omotoso, H. Henein, D.G. Ivey, Metall. Mater. Trans. A **42**, 1767–1784 (2011)
21. A. Paúl, A. Beirante, N. Franco, E. Alves, J.A. Odriozola, in: *Materials science forum*, pp. 500–504. Trans Tech Publications
22. R. Schäublin, P. Spätig, M. Victoria, J. Nucl. Mater. **258**, 1178–1182 (1998)
23. C. Pandey, M. Mahapatra, P. Kumar, A. Giri, Met. Mater. Int. **23**, 900–914 (2017)
24. H. Ma, S.-L. Liao, S.-F. Wang, J. Iron. Steel Res. Int. **21**, 702–709 (2014)
25. W. Choo, J.Y. Lee, J. Mater. Sci. **17**, 1930–1938 (1982)
26. F. Wei, T. Hara, K. Tsuzaki, Metall. Mater. Trans. B **35**, 587–597 (2004)

27. G. Jl, C. Kd, ISIJ Int. **42**, 1560–1564 (2002)
28. T. Depover, K. Verbeken, Corros. Sci. **112**, 308–326 (2016)
29. M. Mohtadi-Bonab, H. Ghesmati-Kucheki, Met. Mater. Int. **25**, 1109–1134 (2019)
30. H. Lee, J.-Y. Lee, Acta Metall. **32**, 131–136 (1984)
31. E.J. Song, S.-W. Baek, S.H. Nahm, D.-W. Suh, Met. Mater. Int. **24**, 532–536 (2018)
32. E. Wallaert, T. Depover, M. Arafin, K. Verbeken, Metall. Mater. Trans. A **45**, 2412–2420 (2014)
33. T. Shintani, Y. Murata, Acta Mater. **59**, 4314–4322 (2011)
34. Z. Cong, Y. Murata, Mater. Trans. **52**, 2151–2154 (2011)